16 The Structure of Liquid Foams

Stefan Hutzler and Wiebke Drenckhan

CONTENTS

16.1 INTRODUCTION

Understanding foam structure is a key to understanding many foam properties. The opacity of a foam, for example, is a consequence of light being scattered from the thin films separating the bubbles or from the Plateau borders where the films meet. The drying out of a foam under gravity is governed mainly by the flow of liquid through the Plateau border network. This network also governs how the electrical conductivity of a foam varies with its liquid volume fraction and how foam flows when sheared (foam rheology, Chapter 7). The existence of a yield stress and the property of shear thinning require an understanding of the structural changes due to bubble rearrangements.

This chapter, which is based on our recent review [1], introduces a number of key descriptors of foam structure, such as liquid volume fraction, bubble mono- or polydispersity or order and disorder. The aim is to introduce the reader to the large range of different types of foam structures that are found in nature or may be produced in the laboratory.

After a brief overview of foam structures (Section 16.2), we will in Section 16.3 justify several approximations that simplify their analysis. Section 16.4 is dedicated to the analysis of dry foams with liquid volume fraction $\varphi < 0.05$, consisting mainly of bubbles with almost polyhedral shapes. Section 16.5 describes experimental studies of wet foams and Section 16.6 concerns the nature of bubble interactions in such foams. Section 16.7 is a brief summary of experimental, analytical, and computational methods for understanding foam structure. A concluding Section 16.8 completes this chapter.

16.2 OVERVIEW OF DIFFERENT FOAM STRUCTURES

The left photograph in Figure 16.1 shows a typical polydisperse, disordered liquid foam under gravity, sitting on top of a liquid pool. The shape of the bubbles in a foam depends on the local liquid fraction φ (the ratio of the liquid volume to foam volume). At the bottom of the foam column, that is, at the foam-liquid interface, the bubbles are nearly spherical. The liquid fraction corresponding to this *wet limit* is around 36%, that is, $\varphi_c = 0.36$, for foams of low polydispersity. This is the value corresponding to the packing fraction $1 - \varphi_c = 0.64$ of a random close packing of equal volume hard spheres (see also Section 16.6).

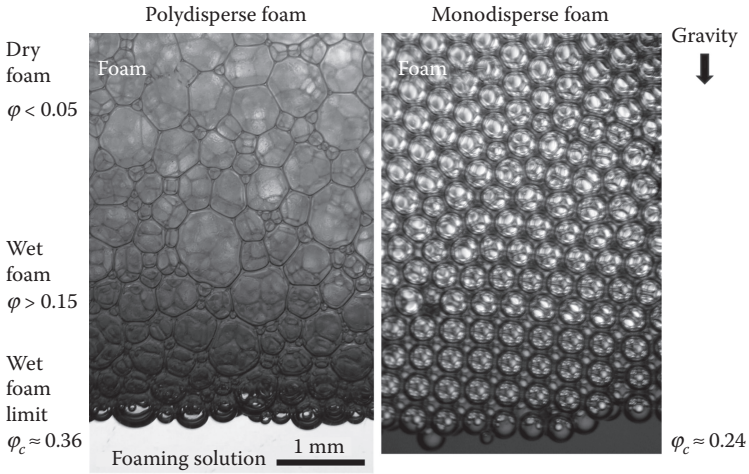

FIGURE 16.1 Photographs of a polydisperse (left) and a monodisperse (right) foam floating on top of the foaming solution. These foams were produced with ordinary dishwashing solution ("Fairy Liquid").

Further up in the foam column, the bubbles are more and more deformed and take on near polyhedral shapes, with thin curved films between them. For liquid fractions $\varphi < 0.05$, we call the foams *dry* (c.f. Section 16.4). Their topology is described by Plateau's rules (Section 16.4). Foams of liquid fraction exceeding about 0.15 are often called *wet* foams, but this value is chosen simply as lying about halfway between the wet and dry limits (see [2]).

Taking this definition of a wet foam, we can estimate its height on top of a liquid pool as $l_c^2/2R$, where R is the mean bubble radius and l_c is the capillary length, given by $l_c = \sqrt{\gamma/\Delta\rho g}$ (γ is the surface tension, g is the gravitation constant, and $\Delta\rho$ is the gas/liquid density difference). The number of bubble layers in this wet foam is called the *Princen number* Pri [3], and it is given by

$$\mathrm{Pri} = \left(\frac{l_c}{2R}\right)^2. \tag{16.1}$$

For a typical foaming solution ($\gamma \approx \gamma_{\mathrm{water}}/2 = 0.036$ N/m), resulting in $l_c \approx 1.6$ mm, the average radius of the bubbles should thus be smaller than 0.25 mm in order to form more than about 10 layers of wet foam.

The polydisperse foam of Figure 16.1 is typical for examples found in nature or many industrial applications. In fundamental research, there is often a preference for studying *monodisperse foams*, consisting of bubbles with a polydispersity of less than 5%. The right photograph in Figure 16.1 shows an example of such a monodisperse foam, again sitting on top of the foaming solution. Such foams have a tendency to order when confined into tubes of width of only a few bubble diameters. They can also order spontaneously in bulk when produced from bubbles that are smaller than the capillary length, resulting in a crystalline wet foam. For more details, see Section 16.5 and [4–7].

In Figure 16.2, we present an overview of different foam structures, emphasizing the role of bubble polydispersity and liquid fraction. Here, polydispersity p_σ is defined via a normalized standard deviation of the bubble radii $R_i = ((3/4\pi)V_i)^{1/3}$ from that of spheres of equivalent volumes V_i,

$$p_\sigma = \sqrt{\frac{<R^2>}{<R>^2} - 1}. \tag{16.2}$$

The polydispersity of foams is generally smaller than 50%, with bubble size distributions depending on the method of foam production [8] (see Chapter 10) or on the age of the foam, since interbubble

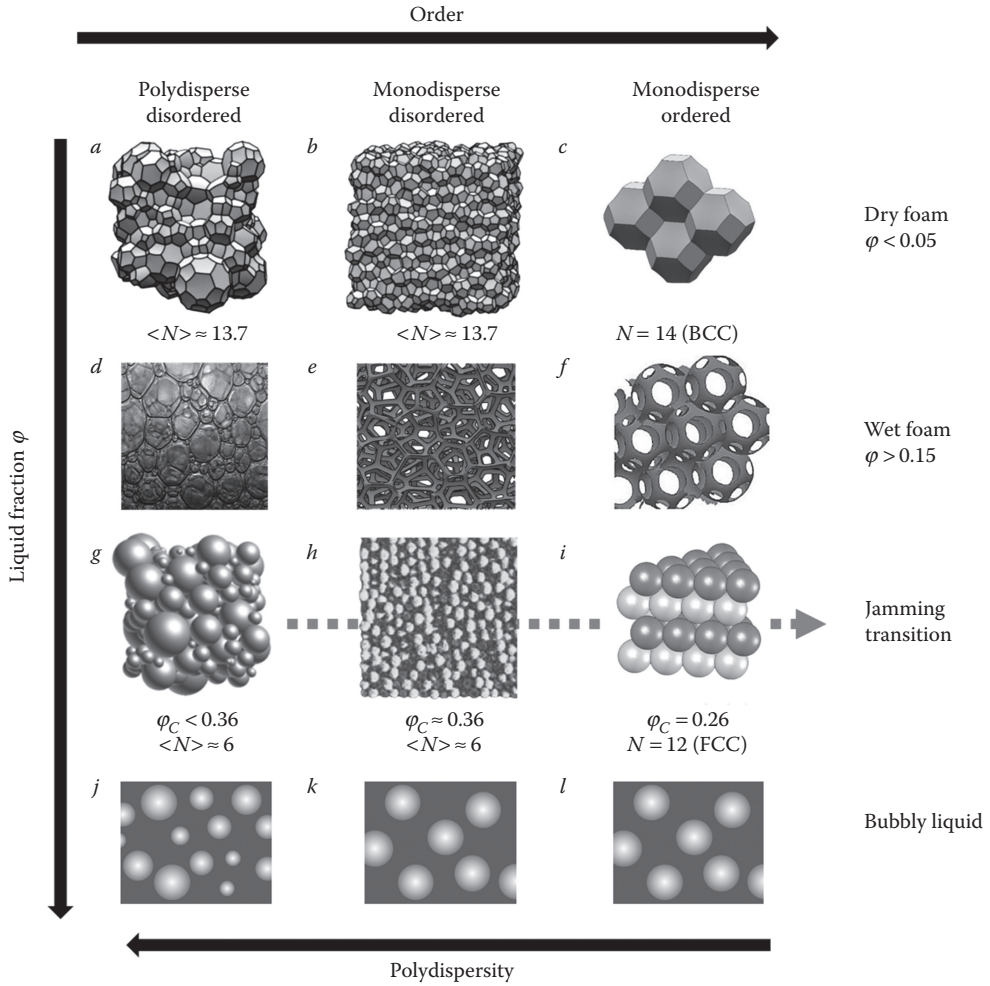

FIGURE 16.2 The structure of a foam depends on liquid fraction φ, polydispersity, and order/disorder. Images: a, b, e, g, thanks to A. M. Kraynik, see also [Kraynik, A.M. et al. *Phys Rev Lett* 2004; 93: 208301–208304 [9]; Kraynik, A.M. *Adv Engineering Materials* 2006; 8: 900–906 [10]]; c and f by S. Cox, see also [Cox, S. et al. In: Scheffler, P.C.a.M. (Ed.) *Cellular Ceramics: Structure, Manufacturing, Properties and Applications*, Wiley, 2005 [11]]; h (Meagher, A.J. et al. Slow crystallisation of a monodisperse foam stabilised against coarsening. *Soft Matter* 2015; 11: 4710–4716. Reproduced by permission of The Royal Society of Chemistry [12]), i (Reprinted with permission from Heitkam, S. et al. Packing spheres tightly: Influence of mechanical stability on close-packed sphere structures. *Phys Rev Lett* 2012; 108: 148302. Copyright 2012 by the American Physical Society.)

gas diffusion will lead to foam coarsening. Film coalescence may also alter the distribution. Foams are called monodisperse if their polydispersity is less than about 5%. It will be shown in Section 16.4 that in some cases, the Sauter mean radius $R_{32} = <R^3>/<R^2>$ is used rather than the average radius $<R>$, so that we can define the polydispersity parameter p_{32} as [9]

$$p_{32} = \frac{R_{32}}{<R^3>^{1/3}} - 1 = \frac{<V>^{2/3}}{<V^{2/3}>} - 1. \tag{16.3}$$

All of this chapter is dedicated to the structure of a foam *in equilibrium*, which is determined by the minimization of surface energy for fixed bubble volumes. In the presence of gravity, this

refers to a foam in which liquid drainage has led to the establishment of an equilibrium profile of liquid fraction (see Figure 16.1). Note that a foam is never in true equilibrium, since processes such as coarsening or coalescence will lead to a further reduction of its energy. It is, however, possible to set up experimental conditions (e.g., using a gas of low solubility, stable surfactants, sufficient environmental humidity, short observation times, etc.) for which a foam may be considered to be *effectively* in equilibrium.

16.3 SIMPLIFYING ASSUMPTIONS FOR UNDERSTANDING FOAM STRUCTURE AND ENERGY

Before describing the structure of dry (Section 16.4) and wet foams (Section 16.5) in greater detail, we will lay out the key simplifications that we make for this analysis. These are

- the surface tension γ is assumed to be constant;
- the bubbles are assumed to be incompressible.

Treating surface tension as constant restricts our analysis to structures in equilibrium in the sense defined above. This means a restriction to times scales which are *sufficiently long* to exceed time scales in which dynamic effects, such as the Marangoni effect (which may play a role in structural relaxation after bubble rearrangements) can be neglected. The time scales must also be *sufficiently short*, so that foam aging effects (coalescence, coarsening) can be neglected. For the discussion of the physicochemistry of foams in relation to foam structure we refer to Chapter 4.

The assumption of incompressibility may be justified as follows. From the Laplace-Young equation we can estimate pressure differences between a bubble of radius R and its surrounding liquid as $2\gamma/R$, where γ is the interfacial tension. For bubbles of radius 0.1 mm and a typical value for γ of 30 mN/m, the resulting pressure difference amounts to about 10^3 Pa. Compared to the atmospheric pressure of 10^5 Pa, this is small enough to consider such bubbles in a foam as incompressible.

The energy of a foam is then simply its total surface energy E, that is, the product of the surface tension γ with the sum of all liquid interfaces S,

$$E = \gamma S. \tag{16.4}$$

For a foam consisting of bubbles with average radius of 0.1 mm, the surface energy is, therefore, of the order of 10^{-8} J per bubble, that is, 10^{13} times larger than the classical thermal energy of $1\ kT \sim 10^{-21}$ J per bubble. In addition, the change in potential energy when vertically displacing a bubble by its radius is proportional to $\Delta\rho g R^4$. This is about 10^9 times larger than kT. Hence, we can conclude that the thermal energy is negligible for the process of packing bubbles.

When comparing (surface) energy of different foam structures, it is convenient to introduce the dimensionless energy $\hat{E}$, defined as

$$\hat{E} = \frac{<S>}{<V>^{2/3}}, \tag{16.5}$$

where $<S>$ and $<V>$ are mean bubble surface area and volume, respectively. For a monodisperse foam consisting of spherical bubbles, this results in $\hat{E} = 3^{2/3}(4\pi)^{1/3} \approx 4.836$. A hypothetic cubic bubble would have $\hat{E} = 6$.

For finite values of liquid fraction, it is often more convenient to introduce the *relative surface excess* $\varepsilon(\varphi)$ as

$$\varepsilon(\varphi) = \frac{<S(\varphi)> - <S_0>}{<S_0>}, \tag{16.6}$$

where $<S(\varphi)>$ is the average total surface area of the foam at liquid fraction φ and $<S_0>$ is the average surface area of the foam, if all its bubbles are treated as spheres. Note that various other related nondimensional quantities are used in the literature.

The energy landscape of a foam is very complex and the bubbles are generally trapped in local energy minima. In the absence of thermal fluctuations, topological changes which would be required to exit such minima, do not occur spontaneously. However, structural changes leading to a decrease of total energy occur as a foam coarsens due to interbubble gas diffusion [2]. They may also be obtained via mechanical shearing of the foam [14] or following the injection of foaming solution into a foam (*forced drainage*). A general consequence of this is that the overall foam structure is strongly history dependent.

16.4 DRY FOAMS

The structure of *dry foams*, that is, foams of liquid fraction of less than $\varphi \approx 0.05$ (Figure 16.2), is well described by Plateau's laws [2,15,16]:

1. Three foam films meet symmetrically under angles of 120° in channels, called Plateau borders.
2. Four such Plateau borders meet symmetrically in a node under tetrahedral angles of *arccos* $(-1/3) \approx 109.47°$ (Maraldi angle).

Plateau's laws are a consequence of the minimization of surface area. They dictate the local topology and geometry of a dry foam. The laws were stated by the Belgian scientist Joseph Antoine Ferdinand Plateau in the 19th century, based on observations of soap films formed in metal wire frames [15].

Most of the liquid in dry foams is contained in the Plateau borders and their nodes. Films of foams in equilibrium are only some tens of nanometers thick and in structural considerations are, therefore, often approximated as having infinitesimal thickness.

The Young-Laplace equation describes the shape of a liquid film between two bubbles having a pressure difference of ΔP as

$$\Delta P = 4\gamma\kappa, \tag{16.7}$$

where κ is the mean curvature of the film surface, given by $\kappa = 1/2((1/r_1) + (1/r_2))$ with r_1 and r_2 as the two principal radii of curvature. The neighboring bubbles in a foam adjust position and shape so as to reach an equilibrium configuration, consistent with Plateau's rules and given bubble volumes.

Computer simulations showed that the pressure in a bubble is correlated with its number of neighbors, which, in turn is correlated with its volume [2,16]. This is important for understanding gas diffusion between neighboring bubbles, called coarsening, disproportionation or Oswald ripening [17].

Equipped with Plateau's rules, in 1887, Lord Kelvin set out to find the equilibrium structure of a monodisperse space-filling foam [18]. His considerations of how space can be divided into equal-size cells with a minimum total interfacial area led him to the shape of a truncated octahedron as the optimal structure (see Figure 16.3 left), consisting of bubbles with $N = 14$ neighbors and arranged in a *bcc* (body-centered cubic) structure [19]. To fulfill Plateau's rules, Kelvin had to introduce a slight curvature into the eight hexagonal faces; the six square faces are flat.

It took more than a century until Weaire and Phelan [20] were able to surpass Kelvin's result by finding a foam structure with 0.3% less interfacial area (see Figure 16.3 right). This so called Weaire-Phelan structure consists of eight equal-volume bubbles, of two different types, and an average number of neighbors of $<N> = 13.5$ [20].

The Weaire-Phelan structure ($\hat{E} = 5.288$) has a lower energy than the Kelvin structure ($\hat{E} = 5.306$). However, due to its complexity, it does not readily form in nature, although it was produced in the laboratory [21].

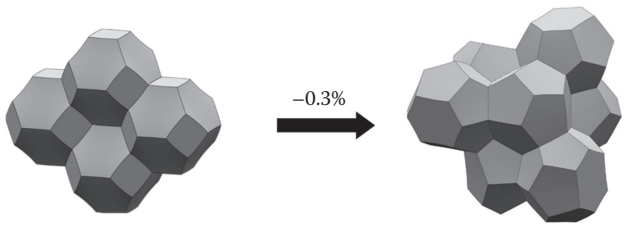

FIGURE 16.3 Surface Evolver simulations of the Kelvin (left) and Weaire-Phelan foam structure, simulations performed by Simon Cox.

Table 16.1 summarizes some of the properties of various dry foam structures. For comparison, the table also includes values for a cubic tiling (which disobeys Plateau's rules) and a hypothetical bubble, with 13.4 faces, whose scaled energy of $\hat{E} = 5.1$ serves as a lower bound [22].

Statistical data about disordered dry foams is mainly based on extensive computer simulations [2,9,10,16,24] using the Surface Evolver software [26]. The left of Figure 16.4 shows the distribution of the number of neighbors of bubbles in foams with different polydispersities. The average number of neighbors of bubbles in a disordered, monodisperse foam is $<N> \approx 13.7$. This is close to the value determined experimentally by Matzke [24] (full circles in the left of Figure 16.4) and to the values for both Kelvin and Weaire-Phelan structures. In polydisperse foams the average number of neighbors decreases with increasing polydispersity.

The right of Figure 16.4 shows that the average number of neighbors of a bubble $<N>$ is correlated with its volume: the larger a bubble is, the more neighbors it tends to have. The simulations also show that with increasing polydispersity, $\hat{E}$ decreases (Figure 16.5).

Furthermore, it was found that each individual bubble in a foam adjusts its shape to obtain a well defined dimensionless energy $\hat{E}^* \approx 5.33 \pm 0.03$ [9], independent of its size [9,27]. This value corresponds to a surface excess of $\varepsilon^*(\varphi = 0) = 0.100 \pm 0.008$ and may be used to calculate how the scaled energy $\hat{E}$ of the entire foam depends on its polydispersity [9] via the relation

$$\hat{E} = \frac{\hat{E}^*}{1 + p_{32}}. \tag{16.8}$$

The line which corresponds to this equation is shown along with the simulation data in Figure 16.5, evidencing excellent agreement.

TABLE 16.1
Summary of Scaled Energy $\hat{E}$ (Equation 16.5), the Relative Surface Excess ε (Equation 16.6), and the Average Number of Neighbors $<N>$ for a Dry Foam ($\varphi = 0$)

Type of Structure	Scaled Energy $\hat{E}$	Relative Surface Excess ε ($\varphi = 0$)	Number of Neighbors N (or $\langle N \rangle$)	Year + Ref
Cubic tiling	6	0.241	6	
Ideal bubble (not space filling)	5.1	0.055	13.4	1992 [23]
Kelvin	5.306	0.097	14	1887 [19]
Weaire-Phelan	5.288	0.093	13.5	1994 [20]
Random monodisperse foam	5.330 ± 0.006	0.102 ± 0.001	13.7	1946/2003 [24,25]
Random polydisperse foam (for $p_{32} < 0.5$) (Equation 16.3)	$3.6 < \hat{E} < 5.33$	0.100 ± 0.008	$11.4 < \langle N \rangle < 13.7$	2004 [9]

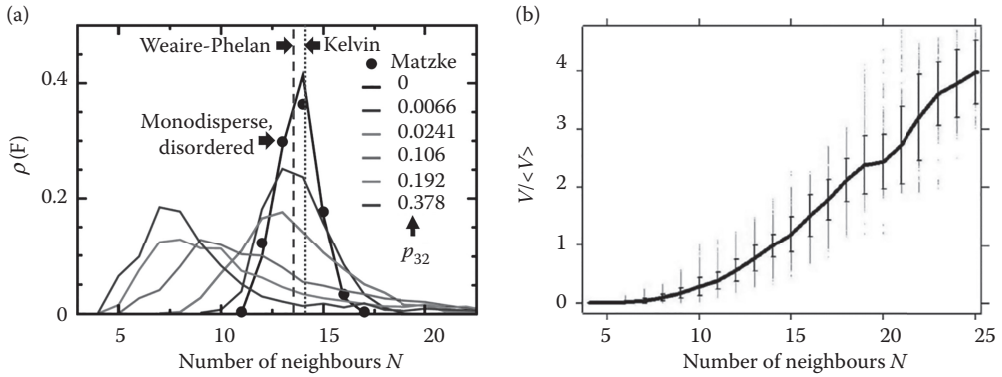

FIGURE 16.4 Left: Probability distribution of neighbors N of bubbles in foams of different polydispersities p_{32}, (•)—experimental data by Matzke [24]; (Reprinted with permission from Kraynik, et al. Structure of random foam. *Phys Rev Lett* 2004; 93: 208301–208304. Copyright 2004 by the American Physical Society [9].) Right: Relationship between the volume of a bubble and its number of neighbors; (Reprinted from *Colloids Surf A*, 263, Jurine, S. et al., Dry three-dimensional bubbles: Growth-rate, scaling state and correlations, 18–26, Copyright 2005, with permission from Elsevier [17].)

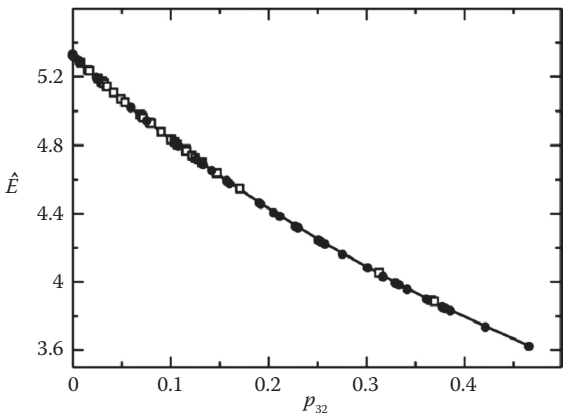

FIGURE 16.5 Scaled energy density $\widehat{E}$ as a function of polydispersity p_{32} for a bidispersive foam (open symbols) and a polydisperse foam (filled symbols); solid line (Equation 16.8) (Reprinted with permission from Kraynik, et al. Structure of random foam. *Phys Rev Lett* 2004; 93: 208301–208304. Copyright 2004 by the American Physical Society [9].)

16.5 EXPERIMENTAL STUDIES OF WET FOAMS

The structure of wet foams is no longer governed by Plateau's laws (see Section 16.4) and 8-fold vertices are possible [28]. Microgravity experiments on soap films spanned by a cubic wire frame showed their stability for a corresponding liquid fraction as low as $\varphi \approx 0.02$ [29]. In earth-bound experiments with ordered bulk foams, Höhler et al. [5] observed a coexistence of a *bcc* structure (with 4-fold vertices) with an *fcc* (face-centred cubic) structure (with 8-fold vertices) at about $\varphi = 0.07$. Simulations with the Surface Evolver agree with this finding. With further increase of the liquid fraction, deviations from the predicted angles at Plateau borders and vertices are also observed, caused by the increasing effective line tension. For more details, see [30].

In order to analyze wet foams experimentally, it is necessary to overcome the drying out of a foam due to gravitationally driven drainage. Several techniques are available for this. The use of bubbles

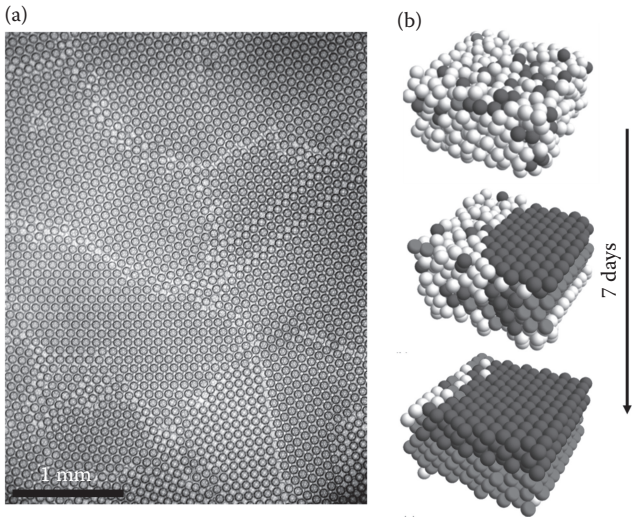

FIGURE 16.6 (a) Photo of the surface of crystalline monodisperse foam, showing different grain orientations, boundaries, and stacking defaults; (van der Net, A. et al. The crystal structure of bubbles in the wet foam limit. *Soft Matter* 2006; 2: 129–134. Reproduced by permission of The Royal Society of Chemistry [4].) (b) X-ray tomography data showing the crystallization of bulk monodisperse foam over the course of seven days. (Meagher, A.J. et al. Slow crystallisation of a monodisperse foam stabilised against coarsening. *Soft Matter* 2015; 11: 4710–4716. Reproduced by permission of The Royal Society of Chemistry [12].)

much smaller than the capillary length, resulting in many bubble layers in the wet regime (large Princen number, Equation 16.1), is one possibility. Alternatively, one may replenish the draining liquid via the addition of a constant flow of surfactant solution at the top of a foam column (*forced drainage* [2]). A third option is provided by experimenting in a microgravity environment [31] (see also Chapter 26).

Surprisingly, monodisperse wet foams consisting of bubbles smaller than a few hundred microns crystallize spontaneously into ordered arrangements. While the ordering is initially confined to regions where the foam is in contact with a confining vessel, or the foam-liquid or foam-gas interface [7,32], as in Figure 16.6a, it has also been seen to occur in the bulk of a sample and to extend in time, as shown in Figure 16.6b [12].

In the ordered regions, it was found that the bubbles arrange in both *fcc* (face centered cubic) and *hcp* (hexagonal close packing), that is, the arrangements associated with the packing of (hard) spheres, with a slight preference for the fcc arrangement. This preference was also found in computer simulations, where the bubbles are treated as soft spheres which aggregate, driven by buoyancy [13]; it was interpreted as a consequence of mechanical stability.

There are yet many open questions regarding the spontaneous ordering in monodisperse wet foams. These include:

- Does coarsening or drainage play a role in restructuring the foam?
- Can mechanical perturbations lead to an annealing of the foam?
- Is the spontaneous ordering a consequence of the specific form of the interaction potential between contacting bubbles, which deviates from that of spheres which interact via Hooke or Hertz contact forces (see Section 16.4)?

16.6 UNDERSTANDING BUBBLE INTERACTION

Rheological measurements and simulations have shown that shear modulus, yield stress, and yield strain decrease with liquid fraction [16,33]. They vanish at the critical liquid fraction close to $\varphi_c \approx 0.36$ ("rigidity loss transition"). In granular materials, this value corresponds to the random packing of

spheres ("Bernal packing") and is also referred to as "jamming fraction" [34,35]. The value of φ_c decreases with increasing polydispersity, but remains close to 0.36 for the modest polydispersities generated by most foaming techniques [8] (Chapter 8). At the jamming transition, the average contact number of bubbles is six, i.e. the value that is obtained from constraint arguments for the packing of frictionless hard spheres [34,35].

Wet foams are often modeled as packings of (overlapping) soft spheres with a pairwise harmonic potential between spheres in contact [34,36]. Computer simulations have shown that this results in an increase ΔZ of the average contact number per bubble of the form $\Delta Z \sim (\Delta\varphi)^{1/2}$, where $\Delta\varphi = \varphi_c - \varphi$ [34].

Although being both computationally and conceptually attractive, the soft sphere model with its fundamental assumption of pairwise-additive interaction energies is only an approximation of bubble interaction. Computer simulations using the Surface Evolver [37,38], as well as analytical studies [39], have shown that the fact that bubbles adjust their shapes upon contact introduces many body coupling between all contacts, together with a logarithmic softening of the interaction. Further studies are required to investigate if and how this affects the scaling of ΔZ with distance $\Delta\varphi$ from the jamming point. Recent computer simulations of two-dimensional foams in which bubble shapes are accurately represented have suggested a linear scaling [40,41].

The Z-cone model presents a novel analytical approach which captures both the logarithmic softening and the dependence of the interaction potential on the number of contacts of a bubble. In the model, a bubble with Z neighbors is decomposed into Z equivalent pieces, followed by their approximation as *circular* cones. Both liquid and gas are treated as incompressible and the minimal surface area of the cap of each cone is computed analytically under the constraint of volume conservation [42,43]. This allows for the computation of the excess energy for periodic foam structures with Z neighboring bubbles as a function of liquid fraction, as

$$\varepsilon(\varphi) \sim -\frac{Z}{18(1-\varphi_c)^2}\frac{(\varphi_c-\varphi)^2}{ln(\varphi_c-\varphi)}, \tag{16.9}$$

in good agreement with simulations obtained with the Surface Evolver in the wet limit [37,42].

While $\varepsilon(\varphi)$ cannot be directly measured experimentally, it can be inferred from measurements of the so called *osmotic pressure* ($\Pi(\phi)$) in a foam, defined as

$$\Pi = -\gamma\left(\frac{\partial S}{\partial V_f}\right)_{V_{\text{gas}}=\text{const.}}, \tag{16.10}$$

where S is the total surface area of all bubbles in the foam of volume V_f, and V_{gas} is the constant gas volume [44–46]. In the case of experimental data for wet ordered foams, the deduced variation for $\varepsilon(\varphi)$ appears to be consistent with the expression obtained from the cone model (Equation 16.9). For details, we refer to our recent review article [1].

16.7 EXPERIMENTAL CHARACTERIZATION OF FOAM STRUCTURE

As we have shown above, foam structure depends crucially on the (local) liquid fraction φ. A number of experimental methods exist for its determination. One of the most elegant methods for measuring the total amount of liquid uses a U-tube filled with foam on one side and the foaming solution on the other side. As the amount of liquid on both sides is equal, the average liquid fraction of the foam can be estimated.

Liquid fraction *profiles* can be obtained via measurements of local electrical conductivity σ, using an array of electrodes in contact with the foam. This technique is based on the well established semi-empirical relationship $\sigma/\sigma_0 = 2\varphi(1 + 12\varphi)/(6 + 29\varphi - 9\varphi^2)$ [47], which expands on the simple

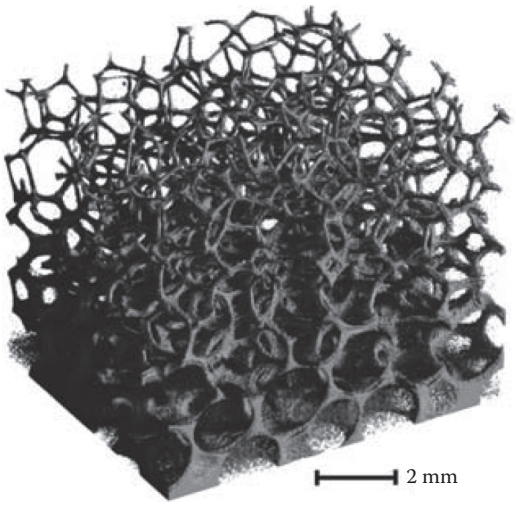

FIGURE 16.7 Tomographic 3D reconstruction of a dry aqueous foam made from ordinary detergent solution and nitrogen bubbles with an average diameter of 1.5 mm; (Meagher, A.J. et al. Slow crystallisation of a monodisperse foam stabilised against coarsening. *Soft Matter* 2015; 11: 4710–4716. Reproduced by permission of The Royal Society of Chemistry [12].)

linear relationship $\sigma/\sigma_0 = \varphi/3$ derived for dry foams by Lemlich [48] (σ_0 is the conductivity of the bulk solution). Various commercial devices are available for such measurements.

Recently, a new technique has been proposed whereby bulk liquid fraction is estimated from optical measurements of the surface liquid fraction of bubbles in contact with a solid confinement [49]. This makes use of semi-empirical expressions of foam excess energy that were referred to in Section 16.6.

The bubble size distribution in a foam may be determined experimentally by placing foam samples between two parallel plates of known separation. The resulting quasi two-dimensional foam can then be analyzed using standard imaging techniques. A rough noninvasive estimation of the average bubble size can also be obtained from photographs of surface bubbles. As in the measurement of the surface liquid fraction, there is the possibility of a bias due to the possibility of size segregation between surface and bulk [50]. A further noninvasive technique is diffusive light scattering combined with a separate measurement of the average liquid fraction [51].

Detailed structural data is hard to obtain. Photography is appropriate only for a few outer layers of foam, but fails as a method for a quantitative analysis of foam structure. The same is true for confocal microscopy. Recently, tomographic techniques, such as X-ray tomography, have proven very successful in determining the Plateau border network and bubble volumes (see Figures 16.6b and 16.7) [12,52,53]. The detection of foam films would benefit from higher energy synchrotron radiation.

16.8 CONCLUSIONS

We have shown that the structure of a foam depends crucially on the method for its generation and on the value of local liquid fraction. The foaming method also controls the degree of polydispersity and introduces the possibility of obtaining ordered, crystalline foams. Bubble shapes range from almost spherical for wet foams to polyhedral for dry foams.

The structure of dry foams is well understood (see Section 16.4) due to the large body of both experimental data and numerical simulations using the Surface Evolver software. This software, developed and maintained by Ken Brakke [26], is presently the most successful tool for simulating foam structure. Example simulations were already shown in Figures 16.2 and 16.3, while Figures 16.4 and 16.5 display Surface Evolver data.

Simulations of disordered wet foams, however, remain challenging, mainly due to the problems associated with detection and execution of topological changes. The Potts model [54,55] provides an alternative Monte Carlo type approach. The recently developed multiscale model of Sethian and Saye [56,57] could also be a candidate for exploring wet foams. Future progress in understanding wet foams will benefit from both advances in experimental imaging, together with new theoretical initiatives, see for example [38].

ACKNOWLEDGMENTS

The work was financially supported by the European Research Council (307280-POMCAPS), the Science Foundation Ireland (13/IA/1926), and by COST Actions MP1106 and MP1305. This work has been published within the IdEx Unistra framework and has benefited from funding from the state, managed by the French National Research Agency as part of the 'Investments for the future' program We would like to thank R. Miller for many suggestions concerning the manuscript.

REFERENCES

1. Drenckhan, W., Hutzler, S. Structure and energy of liquid foams. *Adv Colloid Interface Sci* 2015; 224: 1–16.
2. Weaire, D., Hutzler, S. *The Physics of Foams*. Clarendon Press: Oxford, 1999.
3. Weaire, D., Langlois, V., Saadatfar, M., Hutzler, S. Foam as a granular matter. In: Aste, T., Di Matteo, T., (Eds.), *Granular and Complex Materials*. World Scientific: Singapore, 2007, pp. 1–26.
4. van der Net, A., Drenckhan, W., Weaire, D., Hutzler, S. The crystal structure of bubbles in the wet foam limit. *Soft Matter* 2006; 2: 129–134.
5. Höhler, R., Sang, Y.Y.C., Lorenceau, E., Cohen-Addad, S. Osmotic pressure and structures of monodisperse ordered foam. *Langmuir* 2007; 24: 418–425.
6. Drenckhan, W., Langevin, D. Monodisperse foams in one to three dimensions. *Current Opinion Colloid Interface Sci* 2010; 15: 341–358.
7. Meagher, A.J., Mukherjee, M., Weaire, D., Hutzler, S., Banhart, J., Garcia-Moreno, F. Analysis of the internal structure of monodisperse liquid foams by X-ray tomography. *Soft Matter* 2011; 7: 9881–9885.
8. Drenckhan, W., Saint-Jalmes, A. The science of foaming. *Adv Colloid Interface Sci* 2015; 222: 228–259.
9. Kraynik, A.M., Reinelt, D.A., van Swol, F. Structure of random foam. *Phys Rev Lett* 2004; 93: 208301–208304.
10. Kraynik, A.M. The structure of random foam. *Adv Engineering Materials* 2006; 8: 900–906.
11. Cox, S., Weaire, D., Brakke, K. Liquid foams - Precursors for Solid Foams. In: Scheffler, P.C.a.M. (Ed.) *Cellular Ceramics: Structure, Manufacturing, Properties and Applications*, Wiley: Weinheim, 2005.
12. Meagher, A.J., Whyte, D., Banhart, J., Weaire, D., Hutzler, S., Garcia-Moreno, F. Slow crystallisation of a monodisperse foam stabilised against coarsening. *Soft Matter* 2015; 11: 4710–4716.
13. Heitkam, S., Drenckhan, W., Fröhlich, J. Packing spheres tightly: Influence of mechanical stability on close-packed sphere structures. *Phys Rev Lett* 2012; 108: 148302.
14. Durand, M., Kraynik, A.M., van Swol, F., Kafer, J. Quilliet, C., Cox, S., Talebi, S.A., Graner, F. Statistical mechanics of two-dimensional shuffled foams: Geometry-topology correlation in small or large disorder limits. *Phys Rev E* 2014; 89: 062309.
15. Plateau, J.A.F. *Statique Expérimentale et Théorique des Liquides soumis aux seules Forces Moléculaires*. 2, Gauthier-Villars: Paris, 1873.
16. Cantat, I., Cohen-Addad, S., Elias, F., Graner, F., Höhler, R., Pitois, O., Rouyer, F., Saint-Jalmes, A. *Foams - Structure and Dynamics*, Cox, S. (Ed.) Oxford University Press: Oxford, UK, 2013, p. 300.
17. Jurine, S., Cox, S., Graner, F. Dry three-dimensional bubbles: Growth-rate, scaling state and correlations. *Colloids Surf A* 2005; 263: 18–26.
18. Thomson, W., LXIII. On the division of space with minimum partitional area (Reprinted). *Phil Mag Lett* 2008; 88: A503–A514.
19. Weaire, D. *The Kelvin Problem*. CRC Press: London, 1997.
20. Weaire, D., Phelan, R. A counterexample to Kelvin's conjecture on minimal surfaces. *Phil Mag Lett* 1994; 69: 107–110.

21. Gabbrielli, R., Meagher, A.J., Weaire, D., Brakke, K.A., Hutzler, S. An experimental realization of the Weaire–Phelan structure in monodisperse liquid foam. *Phil Mag Lett* 2012; 92: 1–6.
22. Sullivan, J.M. The geometry of bubbles and foams. In: Rivier, N. Sadoc, J.F. (Eds.), *Foams and Emulsions*, Kluwer: Dordrecht, 1999, p. 403.
23. Kusner, R. The number of faces in a minimal foam. *Proc R Soc Lond, Series A: Math Phys Eng Sci* 1992; 439: 683–686.
24. Kraynik, A.M., Reinelt, D.A. van Swol, F. Structure of random monodisperse foam. *Phys Rev E* 2003; 67: 031403.
25. Matzke, E.B. The three-dimensional shape of bubbles in foam-an analysis of the role of surface forces in three-dimensional cell shape determination. *Am J Botany* 1946; 33: 58–80.
26. Brakke, K. The surface evolver. *Exp Math* 1992; 1: 141–165.
27. Hilgenfeldt, S., Kraynik, A.M., Reinelt, D.A., Sullivan, J.M. The structure of foam cells: Isotropic plateau polyhedra. *Europhys Lett* 2004; 67: 484–90.
28. Brakke, K. Instability of the wet cube cone soap film. *Colloids Surf A* 2005; 263: 4–10.
29. Barrett, D.G.T., Kelly, S. Daly, E.J. Dolan, M.J. Drenckhan, W. Weaire, D. Hutzler, S. Taking Plateau into microgravity: The formation of an eightfold vertex in a system of soap films. *Microgravity Sci Technol* 2008; 20: 17–22.
30. Weaire, D., Vaz, M.F. Teixeira, P.I.C. Fortes, M.A. Instabilities in liquid foams. *Soft Matter* 2007; 3: 47–57.
31. Langevin, D. Vignes-Adler, M. Microgravity studies of aqueous wet foams. *Eur Phys J E*, 2014; 37:16.
32. van der Net, A., Delaney, G.W., Drenckhan, W., Weaire, D., Hutzler, S. Crystalline arrangements of microbubbles in monodisperse foams. *Colloids Surf A* 2007; 309: 117–124.
33. Cohen-Addad, S., Höhler, R. Pitois, O. Flow in foams and flowing foams. *Annu Rev Fluid Mech* 2013; 45: 241–267.
34. van Hecke, M. Jamming of soft particles: Geometry, mechanics, scaling and isostaticity. *J Phys Condensed Matter*, 2010; 22.
35. Lespiat, R., Cohen-Addad, S. Höhler, R. Jamming and flow of random close packed spherical bubbles: An analogy with granular materials. *Phys Rev Lett* 2011; 106: 148302.
36. Durian, D.J. Foam mechanics at the bubble scale. *PRL* 1995; 75: 4780–4783.
37. Lacasse, M-D., Grest, G.S., Levine, D. Deformation of small compressed droplets. *Phys Rev E* 1996; 54: 5436.
38. Hoehler, R. Cohen-Addad, S. Many-body interactions in soft jammed materials. *Soft Matter* 2017; 13: 1371–1383.
39. Morse, D.C. Witten, T.A. Droplet elasticity for weakly compressed emulsions. *EPL* 1993; 22: 549–555.
40. Winkelmann, J., Dunne, F.F., Langlois, V.J., Möbius, M.E., Weaire, D., Hutzler, S. 2D foams above the jamming transition: Deformation matters, *Colloids and Surfaces A: Physicochemical and Engineering Aspects* 2017; 534: 52–57.
41. Dunne, F.F., Bolton, F., Weaire, D., Hutzler, S. Statistics and topological changes in 2d foams from the dry to the wet limit. *Philoso Mag* 2017; 97: 1768–781.
42. Hutzler, S., Murtagh, R., Whyte, D., Tobin, ST., Weaire, D. Z-cone model for the energy of an ordered foam. *Soft Matter* 2014; 10: 7103–7108.
43. Whyte, D., Murtagh, R., Weaire, D., Hutzler, S. Applications and extensions of the Z-cone model for the energy of a foam. *Colloids Surfaces A, Physicochem Eng Aspects* 2015; 473: 115–122.
44. Princen, H.M. The structure, mechanics, and rheology of concentrated emulsions and fluid foams. In: Sjoblom, J. (ed.) *Encyclopedic Handbook of Emulsion Technology*. Marcel Dekker: New York, Basel, 2000, p. 243.
45. Princen, H.M., Kiss, A.D. Osmotic-pressure of foams and highly concentrated emulsions. 2. Determination from the variation in volume fraction with height in an equilibrated column. *Langmuir* 1987; 3: 36–41.
46. Princen, H.M. Osmotic pressure of foams and highly concentrated emulsions. I. Theoretical considerations. *Langmuir* 1986; 2: 519–524.
47. Feitosa, K., Marze, S., Saint-Jalmes, A., Durian, D.J. Electrical conductivity of dispersions: From dry foams to dilute suspensions. *J Phys Condens Matter* 2005; 17: 6301–6305.
48. Lemlich, R. A theory for the limiting conductivity of polyhedral foam at low density. *J Colloid Interface Sci* 1978; 64: 107–110.
49. Forel, E., Rio, E., Schneider, M., Beguin, S., Weaire, D., Hutzler S., Drenckhan, W. The surface tells it all: Relationship between volume and surface fraction of liquid dispersions. *Soft Matter* 2016; 12: 8025–8029.

50. Wang, Y.J. Neethling, S.J. The relationship between the surface and internal structure of dry foam. *Colloids Surf A* 2009; 339: 73–81.
51. Vera, M.U., Saint-Jalmes, A. Durian, D.J. Scattering optics of foam. *Applied Optics* 2001; 40: 4210–4214.
52. Lambert, J., Cantat, I., Delannay, R., Mokso, R., Cloetens, P., Glazier, J.A., Graner, F. Experimental Growth Law for Bubbles in a Moderately ''Wet'' 3D Liquid Foam. *Phys Rev Lett* 2007; 99: 058304.
53. Mader, K., Mokso, R., Raufaste, C., Dollet, B., Santucci, S., Lambert, J., Stampanoni, M. Quantitative 3D characterization of cellular materials: Segmentation and morphology of foam. *Colloids Surf A*, 2012; 415: 230–238.
54. Jiang, Y., Glazier, J.A. Extended large-Q Potts model simulation of foam drainage. *Phil Mag Lett* 1996; 74: 119–128.
55. Thomas, G.L., de Almeida, R.M.C., Graner, F. Coarsening of three-dimensional grains in crystals, or bubbles in dry foams, tends towards a universal, statistically scale-invariant regime. *Phys Rev E (Stat Nonlin Soft Matter Phys)*, 2006; 74: 021407–021418.
56. Saye, R.I., Sethian, J.A. Multiscale modeling of membrane rearrangement, drainage, and rupture in evolving foams. *Science*, 2013; 340: 720–724.
57. Saye, R.I., Sethian, J.A. Multiscale modelling of evolving foams. *J Comput Phys* 2016; 315: 273–301.